Polymer Testing 82 (2020) 106314

Contents lists available at ScienceDirect

Polymer Testing

journal homepage: http://www.elsevier.com/locate/polytest

Material Behaviour

Local process-dependent structural and mechanical properties of extrusion blow molded high-density polyethylene hollow parts

Esther Ramakers-van Dorp [a,b], Benedikt Eger [a], Clemens Raschen [a], Michal Urbanek [c], Bernhard Möginger [a], Berenika Hausnerova [b,c,*]

[a] Bonn-Rhein-Sieg University of Applied Sciences, von-Liebig-Straße 20, 53359, Rheinbach, Germany
[b] Faculty of Technology, Tomas Bata University in Zlin, Vavreckova 275, 76001, Zlin, Czech Republic
[c] Centre of Polymer Systems, University Institute, Tomas Bata University in Zlin, Nam. T.G. Masaryka 5555, 76001, Zlin, Czech Republic

ARTICLE INFO

Keywords:
Extrusion blow molding
Local process-dependent properties
Crystallinity
Complex modulus
Biaxiality

ABSTRACT

Although applied for several decades, production of hollow plastic parts by extrusion blow molding (EBM) is still over-dimensioned. To overcome this issue, a thorough investigation of the process-structure-property relationship is required. In this study, the local process-structure-property relationship for high-density polyethylene EBM containers is analyzed with differential scanning calorimetry and dynamic mechanic analysis micro-indentation. Local process-dependent crystallinity and complex modulus data at various processing conditions are supplemented with wide-angle X-ray diffraction and transmission electron microscopy (TEM). The crystallinities and the complex moduli clearly show lower values close to the mold side than at the inner side and the middle of the cross-section, which reflects the temperature gradient during processing. Additionally, the orientation of the polymer chain (c-axis) reveals a low level of biaxiality with a slight tendency towards transverse direction. The biaxiality increases for low mold temperature and high draw ratio. Finally, biaxiality is confirmed with TEM, which reveals no preferred lamellar orientation.

1. Introduction

Extrusion blow molding (EBM) of hollow plastics, especially high-density polyethylene (HDPE) containers, represents a large segment of the polymer industry. Demands on EBM products are steadily increasing. The EBM process consists of several sequential steps, starting with extrusion of a molten polymer in a vertical direction which results in a parison, followed by clamping two cooled mold halves around the parison, then an inflation of the parison by blowing air into it, and finally, cooling of a final product before demolding [1]. Until today, some issues concerning EBM process still remain unclear and not fully understood. During a parison formation, die swell and sagging affect the wall thickness distribution. Uncontrollable sagging occurs if the parison becomes longer due to gravity. It is influenced by molecular weight distribution, melt strength, extrusion and ambient temperature, and melt relaxation behavior [2–4]. During blowing, the polymer melt is stretched, and an orientation in stretching directions as well as internal stresses after solidification may cause anisotropy, and affect final thermal and mechanical product properties [1]. However, the process-structure-property relationship of EBM products has been so far investigated rarely.

This applies especially for the process-structure-property relationship of HDPE-EBM products in the last three decades. In the early eighties, Kalyon et al. [6] and Kamal et al. [7] studied the parison behavior during EBM to calculate its dimensions and thickness distribution of the molded bottle. They found that for two different PE resins the parison's outer diameter was largest near to the die gap, and the bottle wall thickness was largest near to the bottle bottom. Furthermore, Kamal et al. [8] investigated the thickness distribution, crystallinity, birefringence and impact strength at various positions of an EBM bottle. They concluded that the thickness was greatest near the parting line, while at the top and the bottom of the bottle the thickness was smallest (with a uniform thickness distribution in the middle). The crystallinity distribution was closely associated to the thickness distribution and the cooling rates during molding. The frozen-in stresses and orientations were largest at the outer bottle surface, where the cooling rates were highest. Another interesting study from Kamal and Kalyon [9], where extrusion temperature (200 °C and 225 °C) and inflation pressure (0.46

* Corresponding author. Faculty of Technology, Tomas Bata University in Zlin, Vavreckova 275, 76001, Zlin, Czech Republic.
E-mail address: hausnerova@utb.cz (B. Hausnerova).

https://doi.org/10.1016/j.polymertesting.2019.106314
Received 19 September 2019; Received in revised form 14 November 2019; Accepted 23 December 2019
Available online 25 December 2019

MPa and 0.62 MPa) were varied at a constant mold temperature of 13 °C, showed that a significant anisotropies in the microstructure and material properties occurred due to the heat transfer differences during cooling. Particularly, the crystallinity intended to be higher near the inner side of the EBM bottle, while the frozen-in stresses near the outer side raised up.

Choi et al. [10] reported in the late eighties on the orientation development of polystyrene and polyethylene EBM bottles. They studied the influence of the extrusion temperature (ranging from 160 °C to 200 °C) and the inflation pressure (ranging from 0.10 MPa to 0.42 MPa) on the orientation and concluded low biaxial orientation. They also concluded that the molecular orientation increased with the increasing inflation pressure and the decreasing extrusion temperature. Additionally, their results indicated that the crystallization of the oriented PE melt caused an increase of molecular orientation, and an increase towards biaxiality due to the oriented crystal nucleation and growth.

However, in these studies the influence of the processing parameters on the mechanical properties of the final EBM products was not considered. Thus, recently we investigated the influence of the mold temperature, draw ratio, and the flow direction on the storage modulus and the crystallinity of HDPE EBM containers [11]. All three processing parameters were statistically significant to affect the mechanical properties. Relaxation processes during the samples' storage and the elevated measuring temperatures were considered to explain the intermittent process independency for the flow direction and the draw ratio for specific measuring temperatures from which the mold temperature was unaffected. Furthermore, the mold temperature and the draw ratio showed a significant influence on the crystallinity, where higher mold temperature and higher draw ratio caused higher crystallinities due to the flow-induced orientation. The results were used to improve the reliability of finite element simulations. However, for a further optimization of the simulations, local orientation effects and their influence on the anisotropic material properties is needed [12].

Therefore, in this study the local process-structure-property relationship for EBM containers will be investigated. Process-dependent local crystallinities across the wall cross-section will be analyzed with differential scanning calorimetry (DSC) and process-dependent local complex moduli will be determined with dynamic mechanic analysis (DMA) microindentation. Flow-induced oriented structures will be studied with wide-angle X-ray diffraction (WAXD) and transmission electron microscopy (TEM).

2. Experimental section

2.1. Materials

The polymer used in this study was a commercial HDPE (Lupolen 4261AG, LyondellBasell) with a nominal density of 0.946 g/cm^3 at 23 °C and a mass flow ratio (MFR, 190 °C, 21.6 kg) of 6 g/10 min. Due to its high molecular weight and corresponding viscosity, it is suitable for EBM process [13].

2.2. Processing

Hollow containers were produced on an EBM-machine BFB 2–30 T (Müller Fischer, Germany) by using a special mold that was developed during our preliminary study [12] to obtain a flat sample area (70 × 70) mm with a constant wall thickness distribution (1 mm) and a preset draw ratio for an investigation of mechanical properties. The containers were produced at two different draw ratios (2 and 3.4) and mold temperatures (5 °C and 50 °C) with a constant cooling time of 60 s. The samples are then denoted as e.g. 2/5 reflecting draw ratio/mold temperature, respectively.

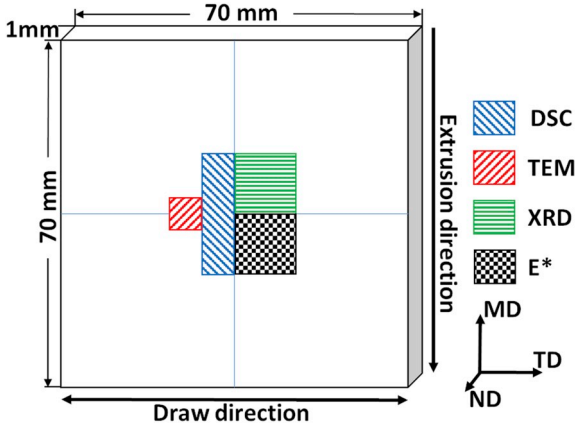

Fig. 1. Outline of sample positions for testing.

2.3. Sample preparation

From the flat sample area, Fig. 1, all specific samples were carefully punched out. The front sample area of the drawing represents the mold side, and the back sample area stands for the inner side of the container after extrusion blow molding. All samples were taken from the middle of the flat sample area to avoid possible variations within the complete flat sample area. Machine direction (MD) corresponds to the extrusion direction, whereas the transverse direction (TD) corresponds to the circumferential direction, perpendicular to the extrusion direction, and the normal direction (ND) is equivalent to the "wall-thickness" direction, perpendicular to the MD and TD planes.

2.4. Characterization

2.4.1. Differential scanning calorimetry

Differential scanning calorimetry (DSC) was used to determine the crystallinity X_{cr} across the wall cross-sections. A 20 μm thick sections (10 × 40) mm across the wall were cut with a microtome (Leica RM 2165, Germany). DSC measurements were performed near the mold and the inner sides every 20 μm, and in the middle of the cross-section every 100 μm. The crystallinity was determined with a DSC 8000 (PerkinElmer, USA). Indium was used as a standard to calibrate temperature and melting enthalpy at a heating rate of 20 K/min in a nitrogen atmosphere. All samples were carefully folded two times and put into aluminum pans (50 μL) to ensure optimum heat transfer during measurement. From the melting enthalpy ΔH_m, measured over a temperature range of −20 °C–180 °C according to EN ISO 11357–3:2018 [14] in a nitrogen atmosphere, the crystallinity was calculated via 3-fold determination with a sample weight about 2.5 mg from

$$X_{cr} = \frac{\Delta H_m}{\Delta H_m^0} * 100\% \quad (1)$$

where $\Delta H^0_m = 293$ J/g [15,16] as a value for 100% crystalline PE.

2.4.2. DMA-microindentation

The newly developed Dynamic Mechanic Analysis microindentation method (DMA-microindentation) [17,18] was used to determine the complex modulus across the wall cross-section. For this, the sample was embedded in a cold curing 2-component epoxy compound (SpeciFix 20, Struers, Germany). After a complete curing, 5 mm thick plane-parallel slice of the embedded sample was cut with an annular saw (SP1600, Leica, Germany) under steady water-cooling to avoid heating during cutting and a consequent possible property changes. Using the x-y-stage, DMA-microindentation measurements were performed (threefold determination) every 100 μm across the cross-section surface, taking at least 2 times indentation-diameter-distance (*2d*) between 2 indentations

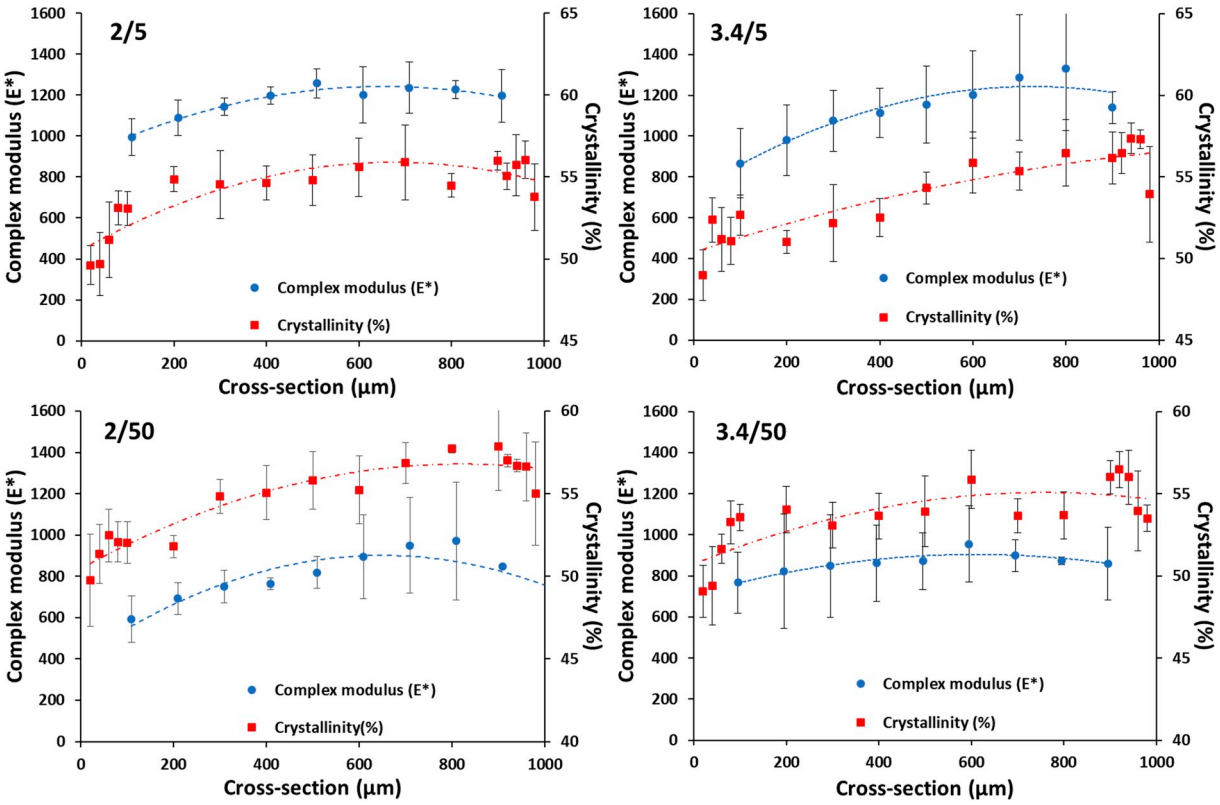

Fig. 2. Process-dependent local crystallinities and complex moduli across the cross-section of the EBM containers (displayed with second order polynomial fits as trendlines for clarity).

into account. *2d* between indentations is needed to avoid material deformation from previous indentations influencing next indentations. A DMA (242C, Netzsch, Germany) was calibrated with a 3 mm flat punch in the standard penetration mode in accordance with the procedure provided by Netzsch. The measurements were performed with a fine tipped tungsten cone indenter at a room temperature at a frequency of 1 Hz, and consisted of two segments. First segment (displacement-controlled) consisted maximum deformation amplitude of 0.10 µm and maximum load of 0.5 N to ensure the initial contact of the indenter with the sample surface, and to set a zero position for the following displacement measurement. Second segment started after reaching an equilibrium state of the first segment. This force-controlled segment was performed with a maximum deformation amplitude of 120 µm and a load of 0.8 N. Both segments were conducted with a so-called proportionality factor of 1.1, where 10% of the dynamic load was used as a static load to ensure the contact of the indenter with the sample surface during the entire measurement. After each measurement, the complex load amplitude F_s^*, the complex displacement amplitude A_s^*, and the penetration depth h were taken to calculate the complex moduli E^* [17,18] from

$$E^* = \frac{F_s^*}{A_s^*} * \frac{(1-\upsilon_s^2)}{2} * \frac{\sqrt{\pi}}{\sqrt{A}} \tag{2}$$

where ν_s is the Poisson's ratio of the sample, and A stands for the contact area.

The contact area A is a function of the displacement h. For the tungsten cone indenter, it can be easily calculated using the trigonometrical function for a cone:

$$A = \pi * tan^2\alpha * h^2 \tag{3}$$

where α is the half opening angle of the cone indenter.

2.4.3. X-ray diffraction

Flow-induced oriented structures in the EBM samples were analyzed by a D8 Discovery (Bruker, USA) with a Vantec 500 2D detector. Wide-angle X-ray diffraction (WAXD) was performed to create pole figures and to calculate orientation factors. From the middle of the flat surface area, Fig. 1, rectangular samples were carefully cut (Leica RM 2165, Germany) to obtain a smooth sample surface. The samples were prepared in both machine (MD) and transverse (TD) directions and mounted on the goniometer. The 2Theta (2θ) measurements were performed with a 0.1 mm collimator using CuK_α radiation produced at 50 kV and 1 mA with a scanning time of 30 s for each step. The diffraction of the lattice planes (110), (200), and (020) of HDPE were analyzed at fixed 2θ angles near to the mold side, sample middle and the inner side of the cross-section. Intensities of these collected patterns were taken at the entire rotation axis of 360° with 10° increments and tilt axis of 80° with 9° increments. These data were used to create pole figures in the software program TEXTURE 4.1 (Bruker, USA) and to calculate the orientation factors using the software EVA 4.1 (Bruker, USA).

The orientation factors for the samples were interpreted from the pole figures in terms of White and Spruiell's biaxial orientation factors defined as [19,20]:

$$f_1^B = 2 * < \cos(\psi)^2 >_1 + < \cos(\psi)^2 >_2 - 1 \tag{4}$$

$$f_2^B = 2 * < \cos(\psi)^2 >_2 + < \cos(\psi)^2 >_1 - 1 \tag{5}$$

where the subscript *1* refers to the machine direction (MD) and the subscript *2* refers to the transverse direction (TD) of the sample.

$< \cos(\psi)^2 >$ is defined as

$$< \cos(\psi)^2 > = \frac{\int_0^{\pi/2} \int_0^{2\pi} I(\psi,\varphi) * \cos(\psi)^2 \sin(\psi) d\varphi d\psi}{\int_0^{\pi/2} \int_0^{2\pi} I(\psi,\varphi) * \sin(\psi) d\varphi d\psi} \tag{6}$$

Table 1
Process-dependent pole figures for the a- and b-axis measured in the machine direction (MD).

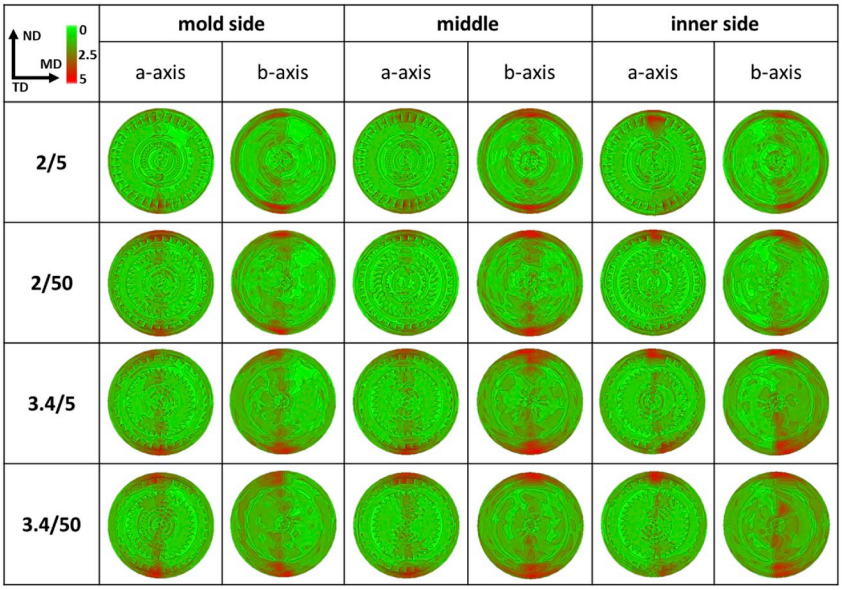

where ψ is the angle between the unit within a crystal of interest and the reference axis, φ is the sample tilt angle, and $I(\psi,\varphi)$ is the intensity diffracted at these angles.

Since the orientation of the c-axis is of main interest and the WAXD-measurement of the c-axis is hardly possible because of the overlap caused by several reflexes from other crystallographic planes, the orientation factor of the c-axis can be indirectly determined based on the orthorhombic unit cell [19,20]:

$$< \cos(\psi)^2 >_{a\,1} + < \cos(\psi)^2 >_{b\,1} + < \cos(\psi)^2 >_{c\,1} = 1 \quad (7)$$

2.4.4. Microscopy

Transmission electron microscopy (TEM) was used to visualize the crystalline lamellae structure near to the mold and the inner side of the sample. The samples were trimmed with a diamond knife installed in an ultra-microtome EM UC7 (Leica, Germany) at low temperature (−120 °C) using liquid nitrogen. The cross-sections of approximately (80–100) nm were subsequently stained for 5 min 10 cm above the damp of a fresh ruthenium tetraoxide solution [21]. TEM was performed on a JEM-2100 microscope (Jeol, Japan) and operated at (120–160) kV.

3. Results and discussion

The performance of EBM products is determined by their structure, including features such as crystallinity and polymer-chain orientation. The anisotropy of the properties is determined by the molecular orientation, which is generally induced during processing and is related to thermo-mechanical behavior of the material. Orientation of polymers might even enhance these properties [1,5].

Fig. 2 shows the local process-dependent crystallinities and the complex moduli across cross-section of all samples, where the cross-section at 0 μm represents the mold side and that one at 1000 μm stands for the inner side. The data is fitted with a second order polynomial to intercept the course across the cross-section.

As it can be seen for all samples, the crystallinities and complex moduli close to the mold side are lower than those in the middle or close to the inner mold side. Due to the EBM processing, where the outer side of the parison cools down during extrusion, and the contact with the cold mold ensures further cooling, fewer crystalline regions were formed in comparison to the position near the mold side. Therefore, lower complex moduli were measured near the mold side. The inner side (near 1000 μm) shows slightly lower values than the middle, but higher than the mold side. Again, this can be explained by the cooling mechanism during EBM processing. Here the inner side experiences different cooling conditions compared to the mold side. During parison formation, the inner side cools down slowly at the ambient air since the heat from the processing is caught within the circular parison and cannot disappear. During blowing of the parison, the inner side is only cooled down by the blown in air, which is a poor heat conductor compared to the metal mold wall. This causes a lower cooling rate than at the mold side, giving the crystalline regions more time to grow. Since no direct cooling can reach the middle of the container wall, even lower cooling rates as on the inner side are reached. Again, this causes higher crystallinities in the middle of the sample, and therefore, higher complex moduli.

Comparison of the mold temperature shows slightly higher crystallinities for (2/50) sample than for (2/5), whereas (3.4/50) sample shows slightly lower crystallinities. A higher draw ratio leads to somewhat higher crystallinity in the case of draw ratio 2; the sample (2/5) compared to the sample (3.4/5), whereas no clear difference in crystallinity can be detected for the samples (2/50) and (3.4/50), Fig. 2. These results indicate that for low mold temperature (5 °C), relaxation processes have not enough time to dissolve the process-induced molecular orientations from which crystallization benefits. At a mold temperature of 50 °C, the relaxation processes are able to dissolve the molecular orientations, so the crystallization becomes dependent on the cooling rate.

A clear difference can be seen for the complex moduli across the cross-section, where the moduli obtained for the lower mold temperature (5 °C) show higher values, than those determined at the higher mold temperature (50 °C). This difference is probably caused by frozen-in thermal stresses originated from higher cooling rates for the mold temperature of 5 °C. Furthermore, a comparison of the draw ratio, 2 and 3.4, reveals only slightly higher complex moduli values for the higher draw ratio attributed as well to internal stresses.

The results from DMA-microindentation across the cross-section of the EBM parts proved to be an advantageous measuring method to determine the process-induced local mechanical properties. This allows a deep inside into the local process-structure-property relationship, and a better correlation of local effects and their influence on the process-

Table 2
Orientation factors of extrusion blow molded samples.

sample	f^B_{1a}	f^B_{2a}	f^B_{1b}	f^B_{2b}	$f^B_{1c}(f_{MD})$	$f^B_{2c}(f_{TD})$
(2/5)						
inner side	0.1210	0.0813	−0.0789	−0.0186	−0.0421	−0.0628
middle	0.1714	0.1505	−0.0053	0.0508	−0.1661	−0.2013
mold side	0.1720	0.1498	−0.0524	0.0085	−0.1196	−0.1583
(2/50)						
inner side	0.1300	0.1012	−0.0990	0.0094	−0.0310	−0.1106
middle	0.1457	0.1015	−0.0603	−0.0207	−0.0855	−0.0808
mold side	0.1188	0.0780	−0.0517	−0.0195	−0.0671	−0.0584
(3.4/5)						
inner side	0.1890	0.1847	−0.0637	0.0384	−0.1252	−0.2231
middle	0.1998	0.1583	−0.0470	0.0521	−0.1528	−0.2104
mold side	0.1876	0.1252	0.0008	0.0767	−0.1883	−0.2019
(3.4/50)						
inner side	0.1481	0.0829	−0.0792	0.0191	−0.0689	−0.1019
middle	0.1730	0.1185	−0.0637	0.0370	−0.1093	−0.1555
mold side	0.1708	0.1104	−0.1171	−0.0283	−0.0537	−0.0821

dependent anisotropic material behavior.

The pole figures for the a- and b-axis measured in MD are depicted in Table 1. Pole figures display preferred crystalline orientation within a sample. From these pole figures it can be seen that both the a- and the b-axis are randomly distributed in the ND-TD-plane, perpendicular to the MD-plane. Additionally, the circular pattern indicates randomly dispersed a- and b-axis around the TD-plane. Thus, from the pole figures no preferred orientation can be concluded.

A comparison with the pole figures measured in TD showed no distinct difference. Caution should be taken regarding the intensity levels from the pole figures since the sample thickness is not constant during WAXD-measurements as the rotating and the tilting angles are changed [22]. Here, even the sample holder can create disturbing diffraction intensity values. Furthermore, a minimum of 3 tilt angles (9°, 46°, and 80°) were used to create the pole figures to reduce data overlap, but still some data overlap was registered as the pole figures were compiled.

The orientation factors for all three axes were calculated (Eqs. (5)–(7)) from the pole figures and summarized in Table 2. All the samples tend to show biaxility

$$f^B_{1a} \approx f^B_{2a}; f^B_{1b} \approx f^B_{2b}; f^B_{1c} \approx f^B_{2c}. \quad (8)$$

Since the c-axis referring to the polymer chain axis is of most interest, these orientation factors are plotted as a White-Spruiell isosceles triangle diagram in Fig. 3. In the triangle diagram, the two corners represent uniaxial orientation in MD for f^B_{1c} (1,0) and TD for f^B_{2c} (0,1), respectively, while the altitude is a state of equal biaxial orientation. The apex (−1,-1) represents the orientation perpendicular to the surface of the sample, in ND [23]. All samples show biaxial orientation of the c-axis, and only a slight orientation towards TD. For extrusion blow molding, orientation in TD is determined by the inflation, and orientation in MD is determined by gravity. Further, it has to be considered for frozen-in orientation that it is necessary to account for relaxation due to cooling of the container after blowing but prior to solidification [20]. The sample with the higher draw ratio (3.4) shows more tendency towards biaxiality, than the lower draw ratio (2) samples.

When comparing these results to the study by Choi et al. [10], clear difference is observed. In their study of extrusion blow molded HDPE bottles, they found a positive biaxial orientation of the c-axis, biaxial orientation in the MD-TD-plane. Furthermore, the pole figures from the a- and b-axes showed a clear orientation along TD and ND, respectively. The differences between the studies can be explained by the variation in processing parameters. Choi et al. [10] produced bottles with different HDPE resin, applied lower extrusion temperatures (200 °C), shorter parison length (the bottles were 12 cm long), and the main influencing difference was the bottle wall thickness ranging from 0.15 to 0.6 mm. For this current study, the extrusion temperature was set on 230 °C, recommended by the polymer supplier. Further, the parison length was about 40 cm to enable the preset draw ratios and the wall thickness of 1 mm within the flat sample area of the extrusion blow molded containers. This means that for this study, the parison needed more time to be extruded, hanging free from the die, enabling the aligned polymer chains (caused by the extrusion) to relax. Furthermore, higher extrusion temperature and thicker container walls caused lower cooling rates, enabling also the aligned polymer chains (caused by the blowing) to relax more resulting in less developed orientations.

Fig. 4 provides an example of transmission electron micrographs for the (3.4/5) sample close to the mold and the inner side, both in MD and

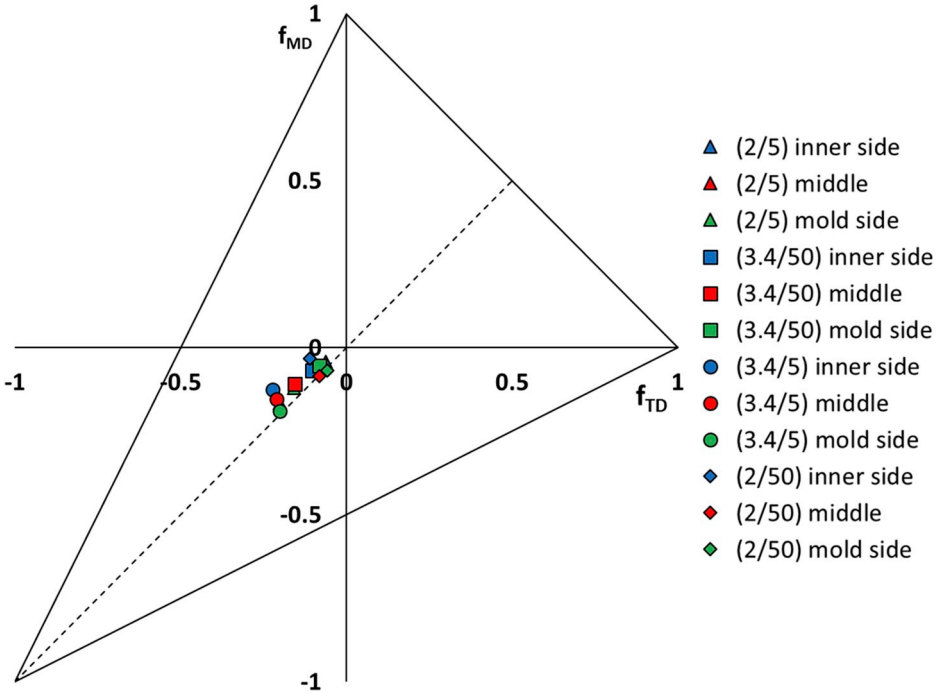

Fig. 3. White-Spruiell isosceles triangle of the c-axis of orientation factors derived from X-ray diffraction.

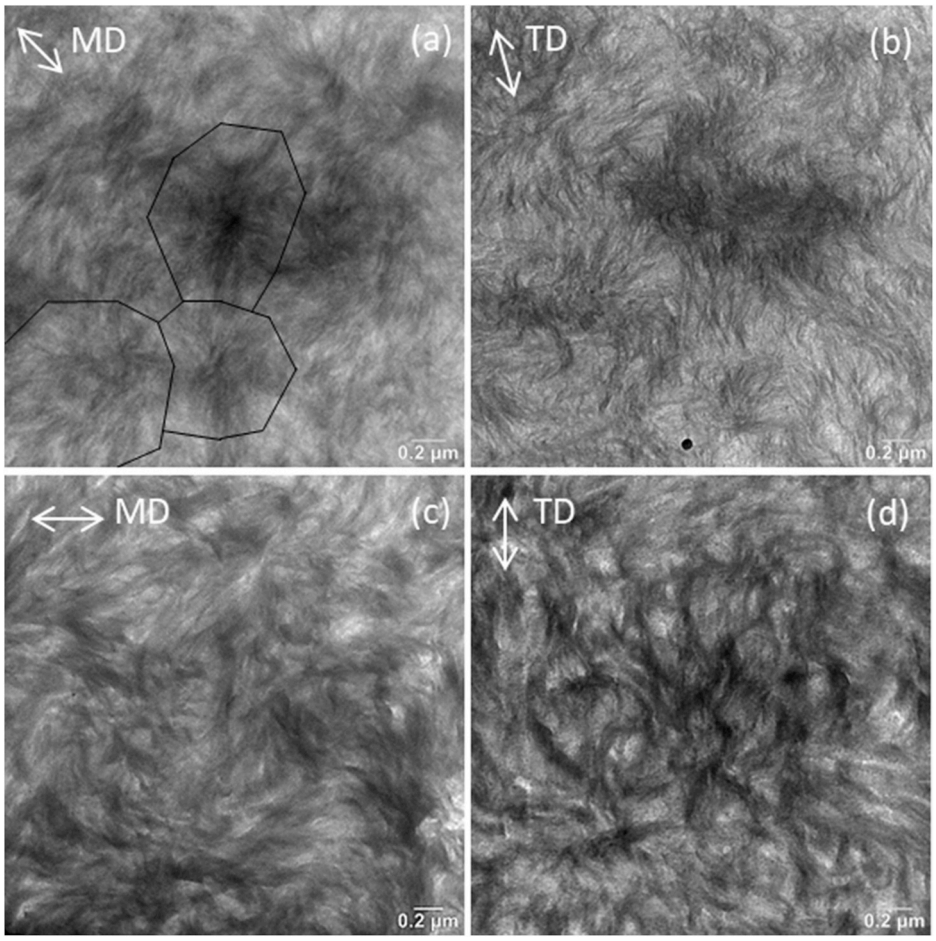

Fig. 4. Transmission electron micrographs of the (3.4/5) sample: (a) parallel to MD close to the mold side, (b) parallel to TD close to the mold side, (c) parallel to MD close to the inner side, (d) parallel to TD close to the inner side.

TD, where the lamellar orientation should be most developed. However, the lamellae in all images, Fig. 4 (a-d), are randomly dispersed in all directions showing no clear lamellar alignment parallel or perpendicular to MD or TD. Since the orientation factor triangle, Fig. 3, showed no clear uniaxial orientation in MD or TD as well, no shish-kebab structures or obvious preferred lamellar orientations is confirmed. In Fig. 4 (a), some spherulites are indicated. They show a circular pattern, which is consistent with isotropy and low levels of biaxiality.

4. Conclusion

Local process-structure-property relationship for high-density polyethylene extrusion blow molded containers was investigated to obtain the precise knowledge of the polymer orientation caused by processing, and the relationship of the resulting structural composure and mechanical behavior, which is crucial for choosing the optimal processing conditions. The local process-dependent crystallinities were analyzed with differential scanning calorimetry and the local process-dependent complex moduli were determined with especially developed dynamic mechanic microindentation. Furthermore, the flow-induced structures were studied with wide-angle X-ray diffraction and transmission electron microscopy. It was shown that (due to the cooling conditions during extrusion blow molding) the temperature gradient across the wall cross-section caused locally different crystallinities and complex moduli. Crystallinities close to the mold side were lower than those located in the inner mold side and the middle of the cross-section, which reflect the temperature gradient during processing. The complex moduli showed a similar trend. Higher values of the complex moduli for the lower mold temperature can be explained by the enhanced frozen-in stresses caused by faster cooling rates. Further, it has been demonstrated that the orientation of the polymer chains (c-axis in X-ray diffraction) revealed low level of biaxiality with a slight tendency towards the transverse direction, which is more pronounced at low mold temperature and high draw ratio. The low level of biaxiality was supported by the transmission electron micrographs, where no preferred lamellar orientation was detected.

This investigation of processing-structure-property relationship should enable extrusion blow molder to predict the physical and the mechanical properties of EBM products leading to an improvement of final products performance.

Declaration of competing interest

The authors declare no conflict of interest.

Acknowledgements

This study was supported by the German Ministry of Education and Research. Grant No.: 03FH051PX4. The author E. R-vD. also thanks the Graduate Institute, Bonn-Rhein-Sieg University of Applied Sciences for supporting this work by granting a scholarship. Special thanks goes to the Dr. Reinold Hagen Foundation, Bonn, Germany, for producing the EBM containers in their technical center and for providing the authors with technical advice. The author B.H. was supported by the Ministry of Education, Youth, and Sports of the Czech Republic - Program NPU I (LO1504).

References

[1] D.V. Rosato, A.V. Rosato, D.P. DiMattia, Blow Molding Handbook, second ed., Hanser, München, 2004.
[2] V.K. Konaganti, M. Ansari, E. Mitsoulis, S.G. Hatzikiriakos, J. Non-Newtonian Fluid Mech. 225 (2015) 94–105.
[3] A. Yousefi, H. Atsbha, Polym. Eng. Sci. 49 (2008) 229–239.
[4] C. Suvanjumrat, N. Ploysook, R. Rugsaj, Eng. J. 22 (2018) 169–183.
[5] D. McKelvey, G.H. Menary, P.J. Martin, S. Yan, Polym. Eng. Sci. 58 (2018) 1516–1522.
[6] D. Kalyon, V. Tan, M.R. Kamal, The dynamics of parison development in blow molding, Polym. Eng. Sci. 20 (1980) 773–777.
[7] M.R. Kamal, V. Tan, D. Kalyon, Measurement and calculation of parison dimensions and bottle thickness distribution during blow molding, Polym. Eng. Sci. 21 (1981) 331–338.
[8] M.R. Kamal, D. Kalyon, V. Tan, Anisotropy and dimensions of blow-molded polyethylene bottles, Polym. Eng. Sci. 22 (1982) 287–291.
[9] M.R. Kamal, D. Kalyon, Heat transfer and microstructure in extrusion blowmolding, Polym. Eng. Sci. 23 (1983) 503–509.
[10] K.-J. Choi, J.E. Spruiell, J.L. White, Orientation and crystalline morphology of blow molded polyethylene bottles, Polym. Eng. Sci. 29 (1989) 463–470.
[11] E. Ramakers-van Dorp, C. Blume, T. Haedecke, V. Pata, D. Reith, O. Bruch, B. Möginger, B. Hausnerova, Polym. Test. 77 (2019) 105903.
[12] D. Grommes, O. Bruch, J. Geilen, Investigation of the influencing factors on the process-dependent elasticity modulus in extrusion blow molded plastic containers for material modelling in the finite element simulation, AIP Conf. Proc. 1779 (2016), 050013-1 – 050013-5.
[13] Technical data sheet, Lupolen 4261AG. https://www.lyondellbasell.com/en/polymers/p/Lupolen-4261AG, 2019. (Accessed 20 June 2019). www.lyondellbasell.com.
[14] EN ISO 11357-3, Plastics. Differential Scanning Calorimetry (DSC) – Part 3: Determination of Temperature and Enthalpy of Melting and Crystallization, 2018.
[15] B. Wunderlich, Thermal Analysis, Academic Press, New York, 1990, pp. 417–431.
[16] D.W. van Krevelen, Properties of Polymers, third ed., Elsevier Scientific Publishing Company, Amsterdam, 1997, pp. 118–127.
[17] E. Ramakers-van Dorp, T. Haenel, F. Sturm, B. Möginger, B. Hausnerova, Polym. Test. 68 (2018) 359–364.
[18] E. Ramakers-van Dorp, T. Haenel, D. Ciongwa, B. Möginger, B. Hausnerova, Polymers 11 (2019) 833–846.
[19] K.-J. Choi, J.E. Spruiell, J.L. White, J. Polym. Sci., Polym. Phys. Ed. 20 (1982) 27–47.
[20] J.L. White, J.E. Spruiell, Polym. Eng. Sci. 23 (1983) 247–256.
[21] J.S. Trent, Macromolecules 17 (1984) 2930–2931.
[22] B.A.G. Schrauwen, L.C. A.v. Breemen, A.B. Spoelstra, L.E. Govaert, G.W.M. Peters, H.E.H. Meijer, Macromolecules 37 (2004) 8618–8633.
[23] J.L. White, M. Cakmak, Adv. Polym. Technol. 8 (1988) 27–61.